TRR
JOURNAL OF THE TRANSPORTATION RESEARCH BOARD

Research Article

Transportation Research Record
2024, Vol. 2678(5) 316–330

DOI: 10.1177/03611981231189495
journals.sagepub.com/home/trr
Sage

Development of a Finite Element Model to Analyze the Lateral Drift of Autonomous Vehicles and Its Impacts on Rutting Depth on Flexible Pavements Under Mixed Traffic Scenarios

Kaidi Liang[1], Zhendong Qian[1], Yuxin Xie[1], and Haibo Wang[1]

Abstract

The continuous development of technologies, including intelligent networking, machine vision, and new energy vehicles, has made autonomous driving vehicles a research focus. Autonomous vehicles significantly affect road performance under mixed traffic flow conditions with their excellent lateral control ability and driving stability. A finite element model is established to analyze the impact of these modes on pavement deformation under maximum air temperature in Nanjing, China. Based on the simulation results, it has been shown that lateral control of autonomous vehicles significantly reduces pavement deformation. The proportion of autonomous vehicles affects the difference in distribution modes, and the uniform distribution mode is the most favorable for horizontal distribution. Additionally, the edge lane experiences less pavement deformation than the center lane and varies more when the distribution pattern changes. By comparing the deformation of the center and edge lanes, the edge lane experiences a significant reduction in deformation under the uniform distribution mode, with a maximum reduction of 73.7%. Comparing the pavement deformation of center and edge lanes under normal distribution mode and uniform distribution mode shows that safe solutions for the lateral distribution of autonomous vehicles depend on the proportion of autonomous vehicles. The optimal driving speed for autonomous vehicles is 80 km/h under the uniform distribution model, while under the normal distribution model it is 90 km/h or 110 km/h. These findings provide a theoretical basis for the lateral control of autonomous vehicles in the future and propose safe solutions for the lateral distribution of autonomous vehicles.

Keywords

freight systems, connected/autonomous commercial vehicle operations, infrastructure management and system preservation, pavement management systems, pavement performance, traffic simulation, automated/autonomous/connected vehicles

Self-driving technology has developed particularly rapidly over the past decade and has become one of the most popular areas of research today, with the global market for autonomous driving expected to grow to 173 billion dollars by 2030 (*1*). Automatic vehicle (AV) refers to a vehicle that is assisted or replaced by human control through automation technology. The Society of Automotive Engineers (SAE) defines different levels of automation, from no automation (Level 0) to fully automated (Level 5, commonly referred to as automatic, autonomous, or driverless vehicles) (*2*). The development of automatic driving technology will have a positive impact on the transportation system in many aspects, including ensuring driving safety, improving road capacity, energy conservation, and emission reduction. Although the current automatic driving technology has made great achievements, it will take a long time to completely replace the human-driven vehicle (HV). Therefore, the mixed traffic flow composed of HV and AV will inevitably exist (*3*).

[1]Intelligent Transportation System Research Center of Southeast University, Southeast University, Nanjing, P.R. China

Corresponding Author:
Kaidi Liang, liangkaidi66@163.com

The significant difference between AV and HV is the position and distribution of the vehicle load. When an HV is running on the road, the wheel track is not a straight track, but there is a certain lateral displacement phenomenon, which is called wheel drift (*4*). Without lateral control, an AV will maintain a lateral position in the center of the lane, generating repeated single point loads, which will lead to faster damage to the road structure. Many studies have already discussed this issue. Chen et al. (*5*) used the finite element modeling method to demonstrate how the reduction of wheel drift of AVs will accelerate the development of rutting, and the increase of driving speed will offset this effect to some extent. Generally speaking, there are two commonly used methods for allocating the lateral position of vehicles, namely, trajectory-oriented method and fatigue damage-oriented method (*6*). For the trajectory-oriented method, a variety of lateral control modes of AV have been proposed and simulated, such as zero distribution mode, uniform distribution mode, bimodal Gaussian mode, Laplace mode, and two-stage uniform mode, among which the uniform mode, bimodal Gaussian mode, and two-stage uniform mode can have a positive impact on the pavement structure (*7–9*). The fatigue damage-oriented method was first proposed by Chen et al. (*10*). The mode of this method is not to control the distribution of vehicle transverse positions preferentially, but to minimize the change of fatigue damage in the lane, so that the pavement damage state in the lane is consistent. In addition to considering the lateral distribution of a single vehicle, some studies also discuss the lateral distribution of AVs in a platoon. Under the premise of automatic control, taking full account of the fuel consumption of the fleet, the air resistance of the queue, and the damage to the road pavement, an AV fleet that can minimize the road surface damage and ensure fuel efficiency is proposed (*11*, *12*).

Previous studies of AV lateral drift have often disregarded the impact on adjacent lanes and assumed that the vehicles will remain close to the distribution of lane lines. However, it has been demonstrated that external forces can cause vehicles to experience varying degrees of slippage when driving. This slippage may lead to vehicles entering adjacent lanes, potentially endangering vehicles in those lanes. Therefore, it is important to consider a safe lateral distance between AVs and lane lines to avoid these safety hazards (*13*). The main challenge when using AVs is to minimize road damage while ensuring safety. One solution is introducing a lateral safety distance. The concept of lateral safety distance was first proposed by scientists in the former Soviet Union, who developed a theoretical model of lane width called the Bolyankov model (*14*). Jiang et al. (*15*) modified the lateral safety distance by investigating vehicle speed and lateral distance between vehicles, and demonstrated the effectiveness of the model. Zhang and Zhang (*16*) constructed an accident rate model for lane width using statistical methods and adjusted the lateral safety distance using the K-means clustering method. However, the impact of introducing lateral safety distance on the lateral distribution design of AVs and resulting changes in rutting performance have not been examined. Therefore, this paper investigates the effects of lateral safety distance on the lateral distribution design of AVs and explores the impact of various lateral control schemes on rutting depth in mixed traffic scenarios. After introducing the topic, we present our design for the lateral distribution of mixed traffic, which includes six potential lateral control modes. We then construct a finite element model to predict rutting depth under different scenarios and discuss and analyze the simulation results. Finally, we conclude with a summary and conclusions of our findings.

Motivation and Scope

Previous research has demonstrated that the usage of autonomous vehicles is bound to have an adverse effect on the physical capacity of roads. When these vehicles are horizontally distributed, they tend to be closely aligned with adjacent lanes. During harsh weather conditions, such as heavy winds, rain, snow, and thick fog, vehicles may experience varying degrees of lateral slippage (*17–19*). Therefore, driving next to the lane line poses significant safety hazards for cars in adjoining lanes. The aim of this article is to analyze the influence of the lateral safety distance of AVs on their lateral positioning pattern and the damage caused to roads in different scenarios. By examining the lateral arrangement of AVs at different penetration ratios and driving speeds, it is possible to reduce road damage while also avoiding disruption to adjacent lanes. This study can contribute to the effective application of autonomous driving technology by presenting novel approaches to the lateral distribution of AVs.

Methods

Based on the introduction of a vehicle lateral distance model, this study constructed a mixed traffic flow lateral distribution model for different vehicle types and AV penetration rates. In addition, a two-dimensional finite element model was used to simulate pavement rutting performance under different scenarios. The following sections describe the model notations and assumptions, the establishment of the finite element model, and the mixed traffic flow lateral distribution model.

Notations and Assumptions

The notations used in this paper are summarized as Table S1 (see Supplementary Materials).

Without loss of generality, the following assumptions are set in this paper.

1. For the purpose of this investigation, it is assumed that all vehicles, including AVs and HVs, remain within their current lane during travel and do not engage in lane-changing behavior.
2. In this study, we assume equal traffic flow between the center and edge lanes.

Finite Element Modeling

Asphalt mixture exhibits significant viscoelastic properties, and its behavior is highly temperature-dependent, particularly at high temperatures (*20*, *21*). Previous studies have demonstrated that finite element software is a powerful tool for modeling the long-term performance of pavements (*22*, *23*). In this study, we used the finite element method and employed the commercial software ABAQUS for the necessary simulations. To ensure the model closely approximates real-world conditions, we introduced the actual temperature field into the pavement structure. Taking into account the continuous variation of material properties with temperature, a rutting analysis model with continuous temperature change was established (*24*). The following subsections summarize the geometric shape and finite element type, material model, climate parameters, load model, and model validation used in the study.

Geometry of the Finite Element Model. In this study, a finite element model is employed to evaluate the pavement response under diverse mixed traffic scenarios. Commercial finite element software, ABAQUS, is utilized for simulation. To investigate the influence of different lateral control modes and the proportion of AVs, a typical flexible pavement structure is chosen and its corresponding finite element model is presented in Figure 1. The width of the model is 3.90 m to mitigate the impact of boundary stress reflection waves, while its thickness is set at 3.0 m. The mesh of the rutting load area is locally refined to enhance the accuracy of capturing the mechanical response under wheel loading. The prescribed boundary conditions comprise lateral horizontal displacement, no horizontal and vertical displacement at the bottom, and full contact between layers.

Material Model. In the past few years, numerous micromechanical models have been developed to simulate

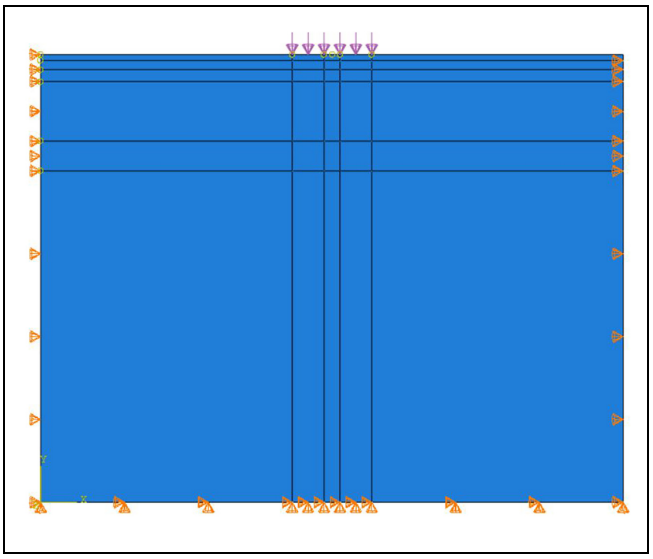

Figure 1. Finite element model of asphalt pavement.

fatigue-induced damage in asphalt concrete. These models include the continuum damage mechanics-based viscoelasticity model (*25*), nonlinear viscoelastic method (*26*), thermodynamically-based nonlinear rate-dependent damage-plasticity coupled particle micromechanical model (*27*), and other approaches. Material creep deformation is the primary cause of rutting, therefore, the Bailey-Norton law is employed for creep deformation analysis in this study (*28*). The model has been widely used and validated for simulating rutting deformation in asphalt layers, demonstrating its soundness and effectiveness (*29*, *30*). Additionally, the tire drift effect on the pavement surface can be taken into account easily by modeling the temporal distribution of tire loading in the transverse direction (*31*). The nonlinear time-hardening creep model enables the determination of the cumulative creep strain, that is, permanent deformation or rutting, and can be characterized by effective stress, equivalent uniaxial creep strain rate, and time, as presented in Equation 1:

$$\varepsilon_{cr} = Aq^n t^m \tag{1}$$

Boundary Conditions of Pavement Temperature Field. The temperature distribution of asphalt pavements is affected by external thermal environmental conditions. However, given the intricacy of the heat transfer process, this study focuses solely on three crucial heat transfer modes: conduction, convective heat transfer, and radiative heat transfer. Based on the fundamental principles of heat transfer, we establish a two-dimensional finite element analysis model. We use the ABAQUS finite element analysis software's user subroutines, DFLUX and FILM, to

define the interaction among heat flow, air temperature, and convective heat transfer with the road surface over time. By this means, we establish a corresponding transient temperature field model to simulate the growth of tire rutting under varying temperature conditions, making the simulation results more realistic (*32*).

The balance of energy on the pavement surface implies that the total heat transfer through the surface of the pavement equals the heat conducted inside the pavement. The temperature field in the pavement is considerably affected by solar radiation and air temperature. Most researchers use the research results of Barber (*33*) to represent the variation of radiant intensity, which can be expressed as follows (*33*, *34*):

$$q(t_n) = \begin{cases} 0 & 0 \leqslant t_n < 12 - \frac{c}{2} \\ q_0 \cos m\omega(t_n - 12) & 12 - \frac{c}{2} \leqslant t_n \leqslant 12 + \frac{c}{2} \\ 0 & 12 + \frac{c}{2} < t_n \leqslant 24 \end{cases} \quad (2)$$

The lowest daily temperature typically appears around dawn, roughly between the hours of 4:00 to 6:00 a.m., while the highest temperature is usually observed approximately 2 h after maximum solar radiation. The time taken for the temperature to increase from the lowest to the highest value is less than 10 h, whereas it takes over 14 h for the highest temperature to decrease to its lowest level. This actual process of temperature change is difficult to simulate with a single sine function, so we propose a linear combination of two sine functions to model the diurnal temperature variation. Our results show that this approach yields good agreement with empirical observations (*35*).

$$T_a = \overline{T_a} + T_m[0.96 \sin \omega(t_n - t_0) + 0.14 \sin 2\omega(t_n - t_0)] \quad (3)$$

The heat exchange coefficient between the road surface and the atmosphere, from thermal exchange, is primarily determined by wind speed. These two factors have a linear correlation (*36*).

$$h_c = 3.7v_w + 9.4 \quad (4)$$

Various factors, such as ground temperature, air temperature, cloud cover, air humidity, and transparency, are closely related to the amount of effective radiation from the road surface. Modifying the surface heat release coefficient or reducing solar radiation can approximate the effect of surface radiation. However, this method is subject to relatively large error. The boundary conditions of effective ground radiation can be directly obtained using the following formula:

$$q_F = \varepsilon\sigma\left[\left(T_1|_{z=0} - T_Z\right)^4 - \left(T_a - T_Z\right)^4\right] \quad (5)$$

Loading Mode and Time. Vehicle loads on asphalt pavement are typically simplified in finite element analysis. Abu Al-Rub et al. (*37*) demonstrated the validity and reasonableness of converting dynamic loads into equivalent static loads. The study converted the number of dynamic load actions into the corresponding number of static load loading times using the following equation.

$$t_0 = \frac{0.36NP}{n_w pBv} \quad (6)$$

Lateral Distribution Design of Mixed Traffic Flow

From a pavement performance perspective, one of the most significant differences between AVs and HVs is the lateral drift of the vehicle. In other words, a computer program can be proposed and developed to design appropriate algorithms for the lateral movement of AVs within their lane, based on theoretical calculations. To ensure that AVs do not cause interference or present any safety hazards to adjacent lanes during lateral movements, a vehicle lateral safety distance model has been introduced. By consolidating various past research, a lateral distribution model is established for mixed traffic flow scenarios and will be further discussed in this chapter.

Lateral Distribution Design of HVs. As a result of the human driver's driving behavior and driving preference, vehicle performance, driving safety, and other factors, the location of each vehicle on the cross section of the lane is random, showing an axisymmetric distribution as a whole. As a result, the vehicle wheel load is concentrated at local points of the cross section of the lane, forming certain lateral distribution characteristics of wheel tracks. To understand the lateral distribution characteristics of HVs, Song and Chen (*38*) collected the lateral distribution of vehicle tires when the vehicle passed over the road. After processing and analyzing the data, it is proved that the lateral distribution of HVs on the road is close to the normal distribution function, and the standard deviation $\sigma = 25$ cm. The lateral distribution probability density function of HVs is as follows (*39*):

$$f_h(x) = \frac{1}{\sqrt{2\pi}\sigma} \exp\left(-\frac{(x-\mu)^2}{2\sigma^2}\right) \quad (7)$$

Lateral Drift Area Model of AVs. Based on the theoretical model of lane width, this study establishes the lateral drift area model of autonomous vehicles at different driving speeds. According to the assumption of the Bolyankov model, the lane width is composed of vehicle width and lateral safety distance. The lateral safety distance can be

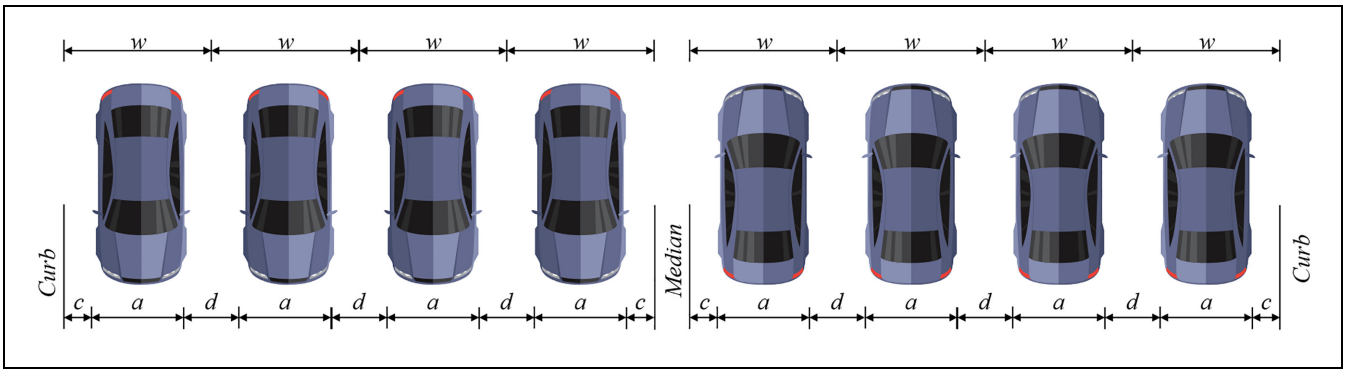

Figure 2. Overview of a divided expressway.

divided into the lateral safety distance of vehicles traveling in the same direction, the lateral safety distance of vehicles traveling in the opposite direction, and the lateral safety distance between vehicles and curbs. The geometric composition of lane width is shown in Figure 2. It is important to note that on a single-direction road segment, the lanes positioned first and fourth from left to right are referred to as edge lanes, while the two lanes in the middle are known as center lanes.

Combined with Figure 1, the Bolyankov model is composed of the following equations (*40*):

$$w_o = d/2 + c + a \tag{8}$$

$$w_i = d + a \tag{9}$$

$$d = 0.7 + 0.02v^{3/4} \tag{10}$$

$$c = 0.4 + 0.02v^{3/4} \tag{11}$$

To make the model more consistent with the current road traffic conditions, Zhang and Zhang (*16*) revised the parameters in the model based on the measured data.

$$d = 0.6 + 0.06v^{0.5} \tag{12}$$

$$c = 0.3 + 0.005v \tag{13}$$

By combining Equations 8, 9, 12, and 13, the theoretical value of the minimum lane width required for the AV to travel safely can be calculated. Then the difference between the actual lane width and the theoretical width is the width of the lateral drift area of the AV, as shown in the following formula:

$$2x_o = w - w_o \tag{14}$$

$$2x_i = w - w_i \tag{15}$$

This AV lateral drift area model is shown in Figure 3.

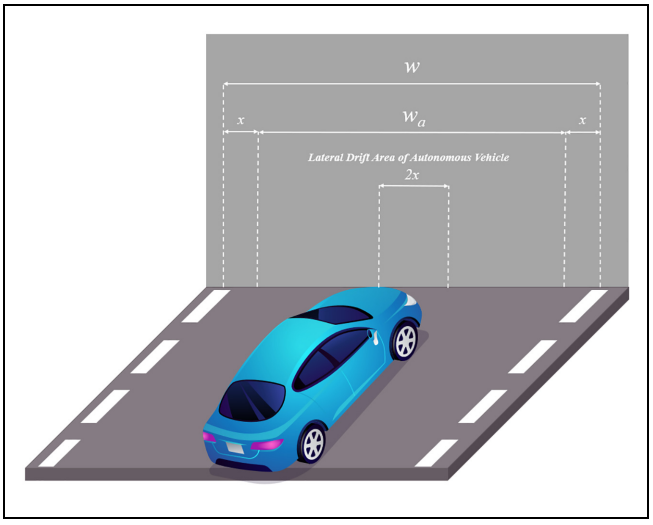

Figure 3. Lateral drift area model of automatic vehicle.

Lateral Distribution Design of AVs. In previous studies, it has been proven that AVs are able to break through many restrictions of HVs, allowing them to behave differently from HVs (*41*). As the lateral distribution of vehicles is closely related to the pavement service life, how to control the lateral distribution of vehicles to extend the pavement service life has become one of the current research highlights. The lateral displacement of the AV is constrained by the dynamic control system and can drift laterally along the given trajectory, which is different from the lateral distribution of HVs. To explore the impacts of the behavior of AVs on the rutting depth under mixed traffic scenarios, three lateral distribution modes, namely zero distribution, normal distribution and uniform distribution, are established in this paper. Zero distribution mode means that the vehicle remains in the center of the lane at all times without lateral drift. This is an extreme scenario, which is set as mode 1. The lateral distribution mode of AVs can simulate the distribution track of HVs, which follows a normal distribution. However, the lateral distribution range of AVs is wider than that of HVs. This method for simulating the distribution trajectory of HVs

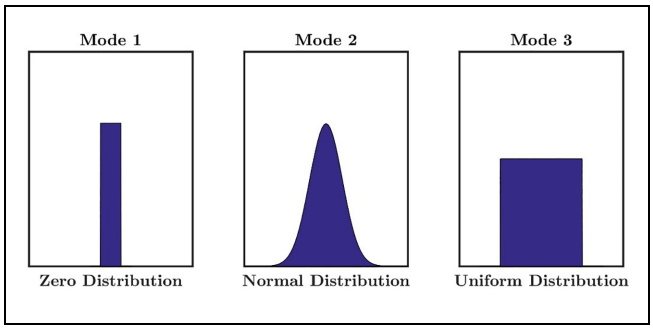

Figure 4. Lateral distributions of automatic vehicles (AVs) under different modes.

is referred to as mode 2. Because of the precise control capabilities of AVs, the lateral positions of AVs can cover the entire drift area evenly, resulting in a more balanced usage of the road surface and less impact on the road; this scenario is mode 3. The lateral distribution of the three modes is shown in Figure 4, and the distribution function is as follows:

$$Mode1 : f_{ai}(x) = f_{a1}(x) = 1 \tag{16}$$

$$Mode2 : f_{ai}(x) = f_{a2}(x) = Norm(\mu \quad \sigma) = \frac{1}{\sqrt{2\pi}\sigma}\exp\left(-\frac{(x-\mu)^2}{2\sigma^2}\right) \tag{17}$$

$$Mode3 : f_{ai}(x) = f_{a3}(x) = U(a \quad b) = \frac{1}{b-a} \tag{18}$$

Lateral Distribution Design of Mixed Traffic Flow. With the introduction of the lateral drift area model, the lateral distribution range of the AV will differ from that of the HV. According to the above model, the lateral drift width of AVs is $2x$, while the lateral drift width of HVs is the whole lane w, as shown in Figure 5. In addition, according to the two conditions of the center and edge lanes, combined with the three lateral drift modes of AVs, the following six combination modes are proposed, as follows:

(a) Edge lane-zero distribution mode
(b) Center lane-zero distribution mode
(c) Edge lane-normal distribution mode
(d) Center lane-normal distribution mode
(e) Edge lane-uniform distribution mode
(f) Center lane-uniform distribution mode.

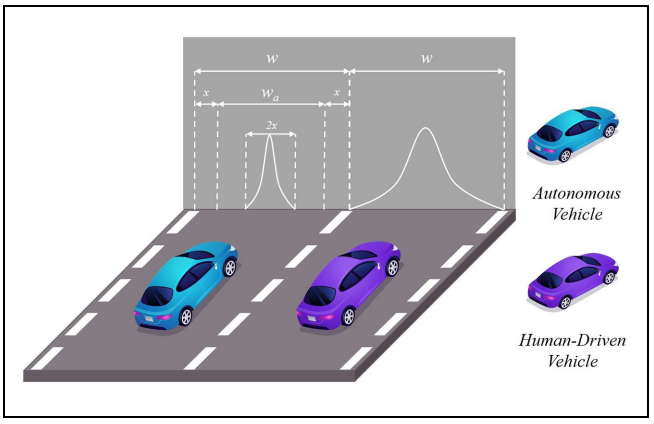

Figure 5. Schematic diagram of vehicle lateral displacement.

Considering that AVs cannot completely replace HVs in the initial stage of development, there will be a mixed traffic flow of HVs and AVs for a long time. When discussing the six combination modes, it is necessary to introduce different proportions of AVs into the lateral distribution design, which results in a composite function for the lateral distribution of the mixed traffic flow.

$$h_i(x) = W \times f_{ai}(x) + (1 - W) \times f_h(x) \tag{19}$$

Case Study

Pavement Design Parameters

This section focuses on the Jiangsu segment of the Shanghai-Nanjing Expressway (China) as the subject of study. Through a comprehensive exploration of pertinent literature and on-site investigations, the relevant information concerning the type of pavement structure, material parameters, and vehicle load parameters has been obtained. This information contributes to forming the basis of developing a finite element model for the Shanghai-Nanjing Expressway.

Pavement Structure and Material Parameters. The Shanghai-Nanjing Expressway is a fully enclosed and interchanged highway; its main technical specifications are presented in Table 1. The typical structure of the pavement is shown

Table 1. Main Technical Indicators of Case-Study Road

Design speed (km/h)	Number of one-way lanes	Lane width (m)	Radius of general circular curve (m)	Minimum radius of circular curve (m)
120	4	3.75	5,500	3,300

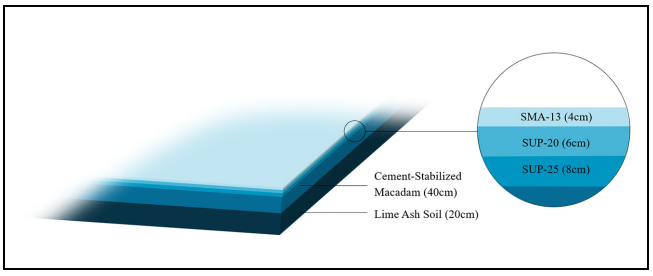

Figure 6. Typical asphalt pavement structure of Shanghai-Nanjing Expressway (China).

in Figure 6, with a 4 cm thick SMA-13 layer on top, a 6 cm thick SUP-20 layer in the middle, and an 8 cm thick SUP-25 layer at the bottom, with a 40 cm cement-stabilized macadam layer and a 20 cm lime soil layer set underneath.

To ensure precise finite element analysis, it is crucial to determine the pertinent parameters associated with each material layer. By referencing relevant research, the material parameters for every layer under varying temperatures have been catalogued in Table 2 as follows (*42, 43*).

Vehicle Model and Load Parameters. This study selected four small cars as research subjects to accurately describe the damage caused by mixed traffic flow on roads. To ensure model representativeness, the design parameters were based on the average values of the vehicle parameters for the four models of small cars, which are shown in Table 3.

The standard axial load of 100 kN and equivalent circular diameter of 21.3 cm for one wheel were used in all six combination modes to ensure a ground pressure of 0.7 MPa. The distance between the two wheels was 31.95 cm. The two-dimensional finite element simulation was simplified to a single-axis, two-wheel, double-rectangular evenly distributed load. The load was rectangular with a width of 15.7 cm and a center distance of 31.95 cm. The ground pressure was 0.7 MPa (*5*, *6*). The parameters of standard axial load are shown in the Table 4.

Climate Parameters. Atmospheric temperatures display significant differences between day and night because of solar radiation, resulting in periodic variations. These periodic patterns can be approximated using cyclical variation boundary conditions (*22*). In this study, an experimental investigation was conduct using the day with the highest daily average temperature recorded in Nanjing throughout the year 2021 (from Janurary 1 to December 31) as the representative temperature. The specific parameters associated with the representative temperature are shown in Table 5.

Table 2. Material Characteristic Parameters of Different Layers

Temp (°C)	A	n	m	Elastic modulus (MPa)	Poisson's ratio
SMA-13					
20	6.536×10^{-11}	0.937	−0.592	870	0.25
30	3.325×10^{-9}	0.862	−0.587	620	0.30
40	1.446×10^{-8}	0.792	−0.577	554	0.35
50	1.390×10^{-6}	0.414	−0.525	530	0.40
60	1.464×10^{-5}	0.336	−0.502	526	0.45
SUP-20					
20	4.580×10^{-11}	0.944	−0.596	910	0.25
30	2.461×10^{-9}	0.796	−0.585	752	0.30
40	3.673×10^{-8}	0.773	−0.570	600	0.35
50	4.802×10^{-6}	0.595	−0.532	440	0.40
60	7.778×10^{-5}	0.384	−0.441	380	0.45
SUP-25					
20	4.590×10^{-11}	0.922	−0.581	1,031	0.25
30	3.461×10^{-9}	0.859	−0.576	900	0.30
40	1.956×10^{-8}	0.830	−0.562	710	0.35
50	1.200×10^{-6}	0.322	−0.522	500	0.40
60	3.755×10^{-5}	0.210	−0.418	390	0.45
Cement-stabilized macadam					
NA	NA	NA	NA	1,200	0.20
Lime ash soil					
NA	NA	NA	NA	810	0.20
Soil foundation					
NA	NA	NA	NA	45	0.35

Notes: NA = not available.

Table 3. Major Parameters of the Vehicle Models

Model	Length (mm)	Width (mm)	Rear tread (mm)
NIO ES8	5,022	1,962	1,672
Model X	5,037	2,070	1,699
Model S	4,979	1,964	1,700
WM Motor W6	4,620	1,847	1,565
Average value	4,915	1,961	1,659

Table 4. Parameters of Standard Axial Load

Standard axial load/kN	Tire contact pressure (Mpa)	Center distance between two wheels (cm)	One wheel's equivalent circular diameter (cm)
100	0.7	31.95	21.30

Table 5. The Representative Temperature parameters in this study

Time (t_n)	Temperature (°C)	Time (t_n)	Temperature (°C)
1	28.9	13	35.9
2	30	14	36.7
3	30	15	36.7
4	30	16	36.7
5	29	17	36.7
6	30	18	36.1
7	30	19	34.2
8	32.5	20	33.6
9	33.8	21	31.5
10	35.1	22	32.4
11	35.8	23	31.8
12	35.8	24	29.1

Model Validation

In this section, a simulation analysis of asphalt mixture rutting is conducted using finite element software. Indoor wheel tracking tests were performed under different experimental conditions to obtain empirical results. A finite element geometric model, consistent with the experiments, is then established to verify the reliability of the finite element model by comparing its simulated results with the experimental data.

Standard Rutting Test. Currently, laboratory testing is the primary method used to evaluate the rutting performance of asphalt pavement materials. Representative experimental methods include the standard wheel tracking test, Hamburg wheel tracking test, French wheel tracking test, and Asphalt Pavement Analyzer (APA) wheel tracking test (*44*, *45*). The rutting performance of the individual layers of the asphalt pavement structure was tested using the standard wheel tracking test method in this study.

Figure 7. Standard rutting test instrument.

To accurately simulate real-world conditions, a series of indoor wheel tracking tests on asphalt mixtures are conducted at a temperature of 30°C. A wheel pressure of 0.7 MPa is selected. A test wheel with a 15 mm rubber layer, a diameter of 200 mm, and a width of 50 mm is used. The test specimens are prepared by using a wheel grinder, resulting in dimensions of 300 mm × 300 mm × 50 mm, and a loading speed of 42 ± 1 cycles per minute. Figure 7 shows the experimental equipment used in this study (*46*).

Validation of Finite Element Model. The wheel tracking test specimens are wrapped in metal molds during the actual testing. To simulate the actual test conditions more accurately, full constraints are applied to the bottom of the model while only horizontal displacement was constrained on the side. Previous studies have shown that finite element analysis results of three-dimensional and two-dimensional (2D) plane models are comparable in simulating wheel tracking of asphalt mixtures. However, using 2D plane models saves significant computational time and memory resources (*47*). Consequently, we developed a 2D plane model of the wheel tracking test specimen to simulate the development of wheel tracking. After inputting the material parameters and loading methods, finite element software was used to examine the wheel tracking development of three types of asphalt mixtures under different temperature and load conditions. By comparing the simulation results with the wheel tracking test outcomes, a comparison graph was obtained, as illustrated in Figure 8.

The graph reveals that the finite element model simulation outcomes are consistent with the experimental findings, indicating that using the creep model for finite element model analysis is an accurate method to simulate the effect of multi-stage loading conditions on wheel tracking deformation of asphalt mixtures. This approach offers flexibility and practicality for simulating wheel

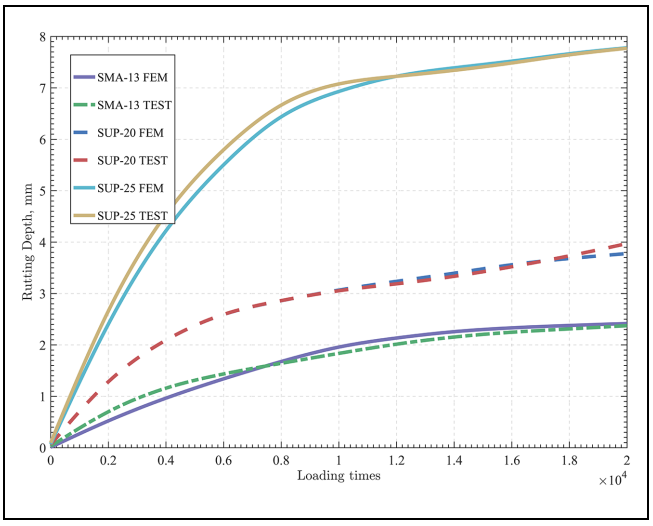

Figure 8. Comparison diagram of standard rutting test and finite element simulation results.

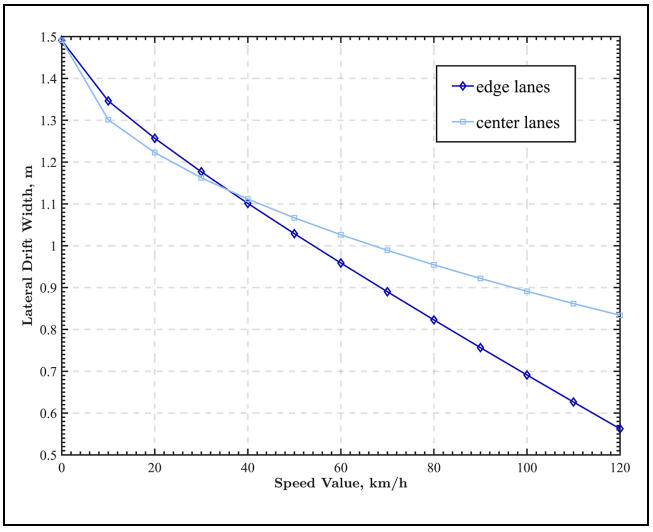

Figure 9. Lateral drift width of edge and center lanes at different speeds.

tracking through finite element model and can aid in further investigating the evolution of wheel tracking in asphalt pavements under complex loading conditions.

Calculation of Lateral Drift Area

This study develops a lateral drift zone model for AVs based on lane width theory, covering various travel speeds. The research focuses on an eight-lane highway featuring a central reservation strip. The setting of the central reservation strip eliminates the impact of oncoming traffic, allowing for the classification of the four lanes into center and edge lanes. The results of the computational analysis, as depicted in Figure 9, are obtained on entering the relevant parameters into the theoretical model of lane width.

The graph illustrates a difference in lateral drift width between the edge and center lanes based on speed, which is explained by the distinct sensitivity of speed changes in these two lanes. Specifically, at low speeds, the center lane has a smaller lateral drift width than the edge lane, while this trend reverses as speed exceeds 40 km/h, reaching its maximum difference at 120 km/h. Notably, the formula indicates that both "d/2" and "c" influence the edge lane, while only "d" affects the center lane, resulting in different ranges of lateral displacement between the two lanes at different speeds. Additionally, as speed increases, the lateral drift distance decreases progressively. However, since the Shanghai-Nanjing Expressway is designed with a speed limit of 120 km/h, further increases in speed are not considered in this analysis.

When analyzing mixed traffic flows, the representative speed for HVs is usually taken as 85% of the road's designed travel speed (i.e., 102 km/h) (*48*, *49*). However, very low speeds significantly affect the prediction results of tire tracks in finite element analysis for autonomous vehicles. Moreover, such slow speeds do not exist in practical traffic situations. Therefore, the cruising speed of autonomous vehicles is set to be between 40 km/h and 120 km/h.

Results and Discussion

Influence of Lateral Distribution of Mixed Traffic Flow on Rutting Development

Many previous studies have compared the rutting depth under zero, normal, and uniform distributions, demonstrating that the uniform distribution mode has the least damage effect on the road. According to Chen et al. (*6*), the uniform distribution mode is the best control mode, which can reduce the fatigue damage by 35%, and delay maintenance by up to 2.3 years compared with expectations. In addition, Yeganeh et al. (*8*) demonstrated that different proportions of AVs caused variability in rutting damage, and the differences under higher proportions were more significant than those under lower proportions. In this study, a lateral drift area model of AVs is introduced to improve safety, and the rutting development of different distribution modes under the influence of this model is simulated. Figure 10 shows the rutting development under different distribution modes.

As shown in Figure 10, the rutting depth in the zero distribution mode is significantly greater than that in the normal distribution mode and uniform distribution mode. In addition, the proportion of AVs in the mixed traffic flow also has an impact on rutting development, with a greater proportion of AVs bassociated with more

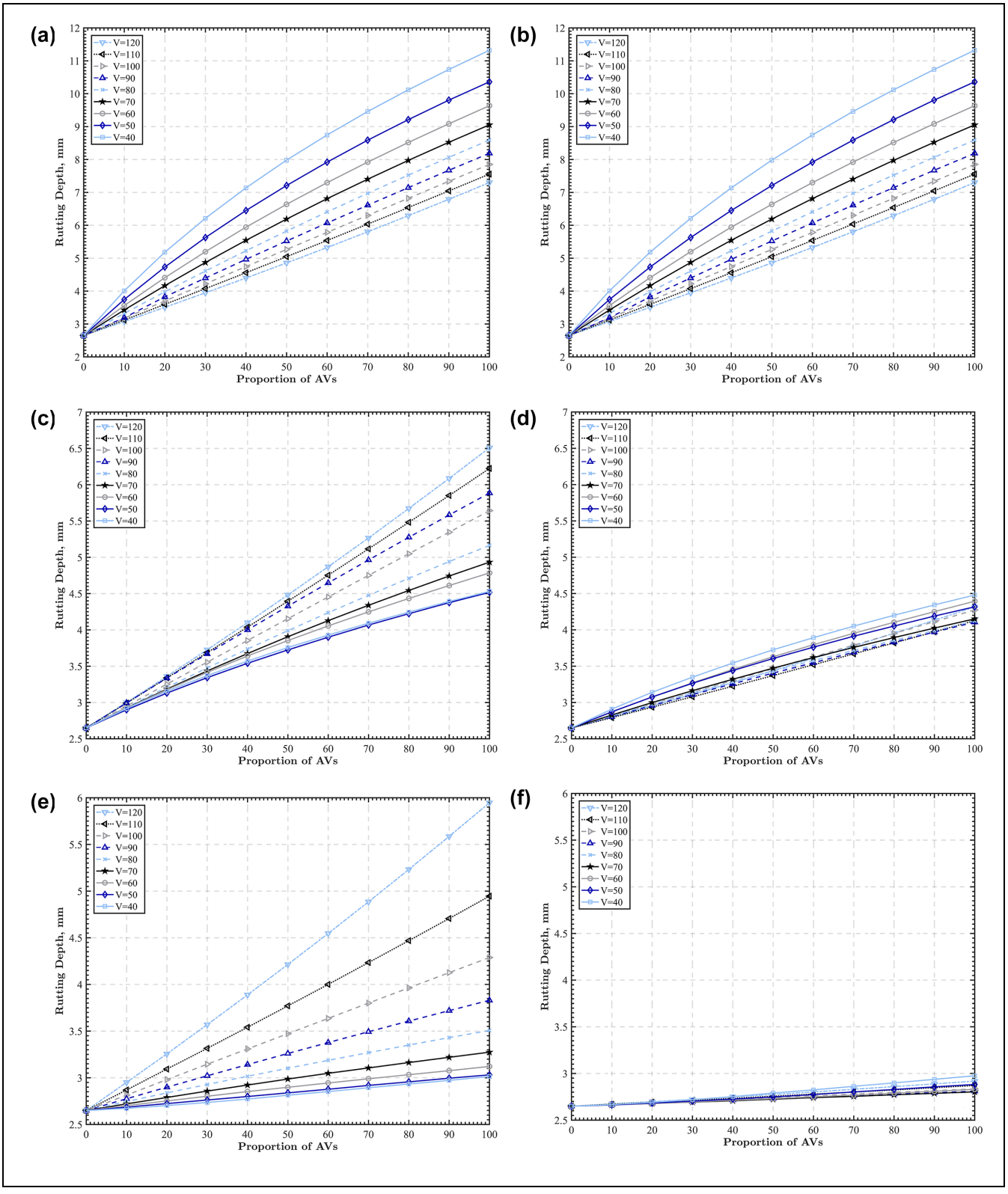

Figure 10. Rutting depth curves under different distribution modes: (*a*) edge lane-zero distribution mode, (*b*) center lane-zero distribution mode, (*c*) edge lane-normal distribution mode, (*d*) center lane-normal distribution mode, (e) edge lane-uniform distribution mode, (*f*) center lane-uniform distribution mode.

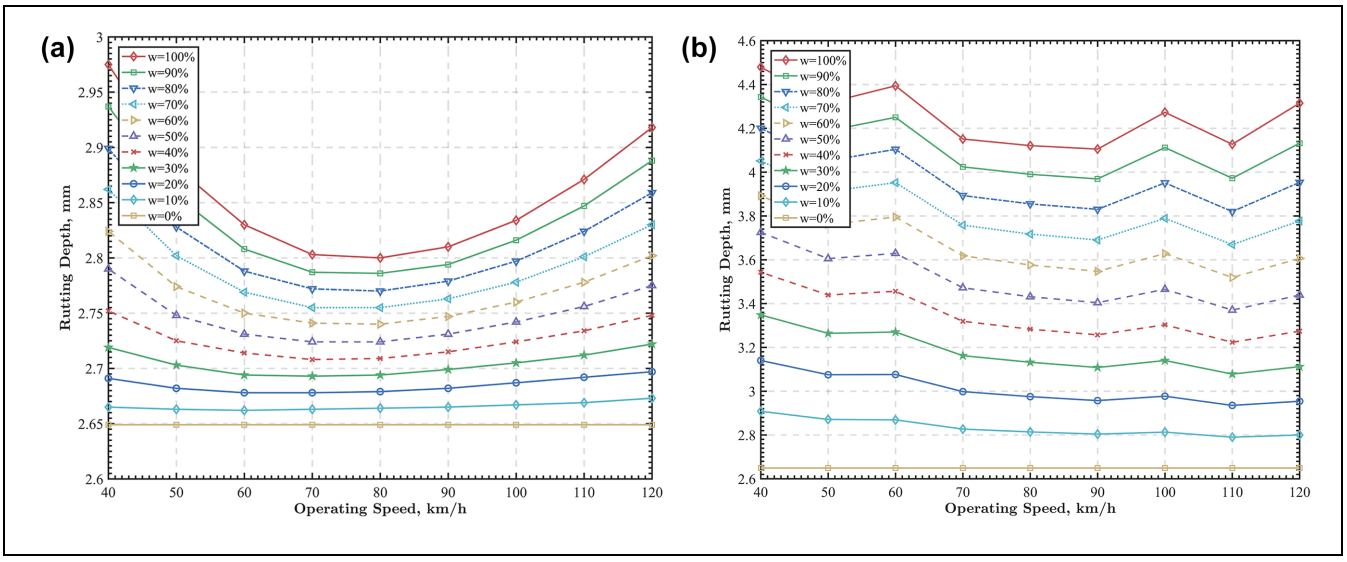

Figure 11. Rutting depth development pattern of center lane for: (*a*) uniform and (*b*) normal distribution modes.

significant variability in the different distribution modes. These findings are consistent with previous studies. However, there are still some differences in these conclusions when the center and edge lanes are analyzed separately.

Although the rutting depths of both center and edge lanes are affected by the changes of distribution mode, the magnitude of the change in rutting depth that occurs when the distribution mode changes vary between the center and edge lanes. Rutting depths are generally greater in the edge lane than the center lane. As shown in Figure 7, the rutting depth of the edge lane changes more significantly, while the rutting depth of the center lane changes slightly. The maximum rutting depth for both the center and edge lanes in the zero distribution mode is 11.320 mm. The maximum rutting depth for the center lanes in the normal and uniform distribution modes is 4.479 and 2.975 mm respectively, a reduction of 6.841 mm and 8.345 mm compared with the maximum rutting depth in the zero distribution mode. However, the maximum rutting depth for the edge lanes in the normal and uniform distribution modes is 6.509 mm and 5.946 mm respectively, a reduction of 4.811 mm and 5.374 mm compared with the maximum rutting depth in the zero distribution mode respectively.

A comparison of the rutting depth variation values for the center and edge lanes shows that the rut depth of the center lane is significantly reduced in the uniformly distributed pattern by up to 73.7%, while the edge lane is only reduced by up to 47.5%. Therefore, AVs should be allowed to drive along the edge lane in uniform distribution mode as far as possible, but the proportion of AVs should not be too high, after taking into account vehicle safety considerations.

Rutting Depth Development Pattern of Center Lane Under Normal and Uniform Distribution Mode

As the safety of AVs when performing lateral distribution has been largely disregarded in previous studies, the issue of center and edge lane variability does not exist. In this study, the lateral drift area model for AVs was established and introduced so that the rutting development patterns of the center and edge lanes in the same scenario differed. As the rutting development trend of the center and edge lanes in the zero distribution mode is the same, only the development trend of the center lane rutting depth in the normal and uniform distribution modes is compared and analyzed, as shown in Figure 11.

The figure shows a distinctive "U" shape representing how the rutting depth in the center lane first decreases and then increases in response to AV cruising speed in both normal and uniform distribution modes. This phenomenon can be attributed to the influence of two factors: vehicle speed and lateral drift width of the road. Specifically, at higher speeds, the lateral drift width of the vehicle decreases, resulting in a more concentrated vehicle distribution and a consequential increase in the depth of ruts. In contrast, at lower speeds, vehicles have a longer dwell time, and an increase in load action time will significantly increase the rutting. Thus, the combination of these two competing factors generates the observed "U" shape. However, there are still some differences in the rutting development patterns between the different distribution modes.

Although the rutting trends are more or less the same for the different distribution patterns, the uniform distribution pattern has a smoother rutting depth trend and is more significantly influenced by speed, with a clear

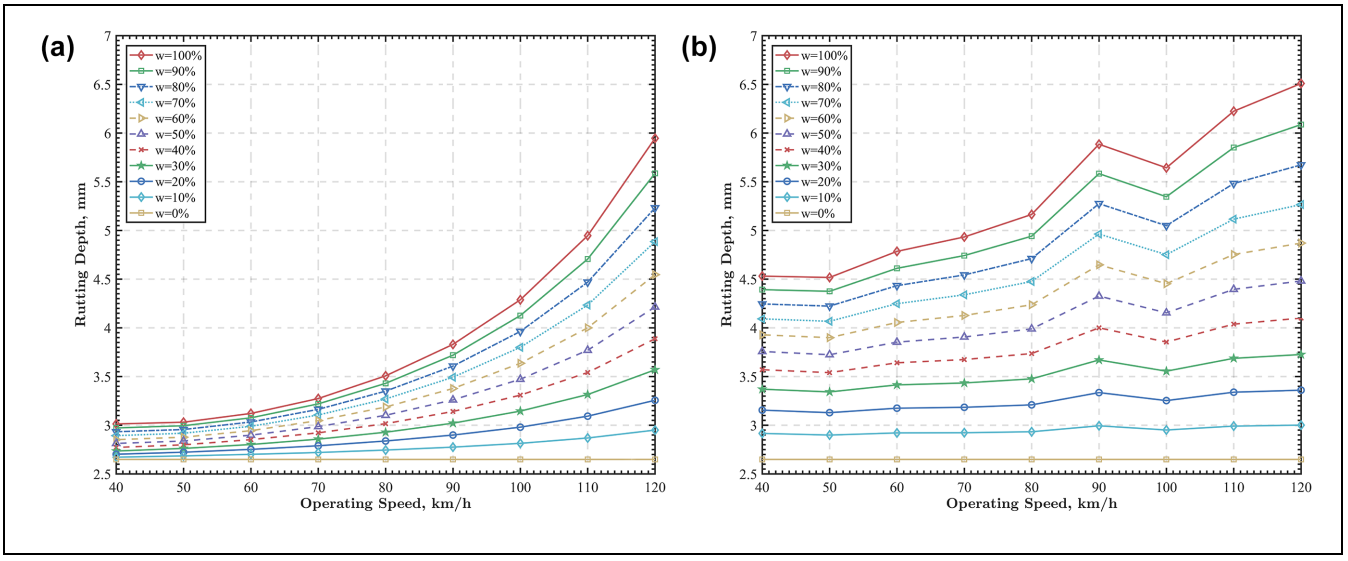

Figure 12. Rutting depth development pattern of edge lane for: (*a*) uniform and (*b*) normal distribution modes.

optimum driving speed. It is observed that the optimal driving speed for AVs in the uniform distribution mode is 80 km/h, and when AVs drive at that speed, they cause the least damage to the road surface. The rutting trend in the normal distribution model is more complex, with the optimum speed being 110 km/h when the proportion of AVs is less than or equal to 80% and 90 km/h when the proportion of AVs is more than 80%. In addition, the rutting depth in the uniform distribution model is overall less than that in the normal distribution model, a finding that is also consistent with the findings in the above contents.

Therefore, when an AV is driving in the center lane, the lateral distribution should be designed according to the uniform distribution pattern as far as possible and the cruising speed should be set at 80 km/h. When the lateral distribution is designed according to the normal distribution pattern, the cruising speed should be adjusted according to the proportion of the autonomous vehicle.

Rutting Depth Development Pattern of Edge Lane Under Normal and Uniform Distribution Mode

As the rutting trends for the center and edge lanes are the same in the zero distribution mode, only the rutting depth trends in the edge lanes in the normal and uniform distribution modes are compared and analyzed, as shown in Figure 12.

As shown in Figure 12, the rutting depth of the edge lane increases with the increase of the cruise speed of AVs, both in the normal distribution mode and in the uniform distribution mode. However, there are still some differences in the rutting development patterns between the different distribution modes.

Although the rutting depth is positively correlated with the speed of AVs in both distribution modes, the sensitivity to speed variation differs, and the rutting depth variation curve is smoother under uniform distribution. As can be observed from Figure 12, when the traffic flow is composed entirely of AVs, the maximum and minimum rutting depths under the normal distribution mode are 6.509 mm and 4.531 mm respectively, with a variation of 1.978 mm. The maximum and minimum rutting depths under the uniform distribution mode are 5.946 mm and 3.013 mm respectively, with a variation of 2.933 mm.

Conclusions

With the aim of improving safety during lateral distribution, a lateral drift zone model for autonomous vehicles was developed and various distribution patterns of mixed traffic flow based on this model were proposed. Based on data analysis, wheel drift significantly affects the fatigue cracking and rutting performance indicators of asphalt layers in flexible pavement. The main conclusions drawn from this survey are as follows:

1. This study proposed three AV lateral distribution modes: zero, normal, and uniform. Comparison of rutting development in these modes demonstrated that the uniform distribution pattern resulted in the smallest rutting depth. The proportion of AVs had a significant impact on variability in the different distribution modes. Rutting depth was generally greater in the edge lane than in the center lane, and varied more significantly when the distribution pattern changed. The maximum relative difference in rutting depth under

the same scenario was 50%. Comparing rutting depths between center and edge lanes, it was found that the uniform distribution pattern significantly reduced rutting depths in the edge lanes by up to 73.7%, while reducing the center lanes by only up to 47.5%.

2. The rutting depth in the center lane exhibits a "U" shaped trend as the cruising speed of AVs increases in both normal and uniform distribution modes, with an optimal driving speed. In the uniform distribution mode, this trend is smoother, and the optimal driving speed is 80 km/h. In the normal distribution mode, the rutting trend is more complicated, with an optimal speed of 110 km/h when the proportion of AVs is less than or equal to 80%, and 90 km/h when the proportion of AVs is greater than 80%.
3. Comparison of rutting depth development in the edge lane under normal and uniform distribution modes shows that increasing cruising speeds result in increased rutting depth. In the uniformly distributed model, rutting depth shows a stronger correlation with speed, with a maximum variation of 2.933 mm.

In this article, the establishment of the AVs lateral drift zone model improves the safety of mixed traffic flow and provides new ideas for the design of lateral distribution in mixed traffic scenarios. Specifically, it demonstrates how to adjust lateral distribution to minimize impact on adjacent lanes while maintaining road surface quality. Clearly, safety is the primary factor to consider in future mixed traffic flow scenarios. This method also provides a theoretical basis for practical projects such as intelligent long-distance freight and unmanned public transportation systems. However, the impact of lateral drift of AVs on the behavior of surrounding vehicles is still unclear, and research on the safety of lateral distribution of AVs remains incomplete. Further study is necessary to design a more accurate and scientific lateral distribution model of mixed traffic flow.

Acknowledgments

The authors would like to express their sincere gratitude to the members of the Intelligent Transportation System Research Center of Southeast University, for their invaluable assistance in developing and interpreting the modeling results presented in this paper. In particular, we would like to thank Professor Chen, Professor Hu, and Bangyan Hu for their valuable contributions and insights. Their guidance and support have been instrumental in enabling us to complete this research.

Author Contributions

The authors confirm contribution to the paper as follows: study conception and design: K. D. Liang, Z. D. Qian, Y. X. Xie; data collection: K. D. Liang, Z. D. Qian; analysis and interpretation of results: K. D. Liang, Z. D. Qian, Y. X. Xie, H. B. Wang; draft manuscript preparation: K. D. Liang, H. B. Wang. All authors reviewed the results and approved the final version of the manuscript.

Declaration of Conflicting Interests

The author(s) declared no potential conflicts of interest with respect to the research, authorship, and/or publication of this article.

Funding

The author(s) received no financial support for the research, authorship, and/or publication of this article.

Supplemental Material

Supplemental material for this article is available online.

References

1. Chakraborty, S., D. Rey, M. W. Levin, and S. T. Waller. Freeway Network Design with Exclusive Lanes for Automated Vehicles Under Endogenous Mobility Demand. *Transportation Research Part C: Emerging Technologies*, Vol. 133, 2021, p. 103440. https://doi.org/10.1016/j.trc.2021.103440.
2. Narayanan, S., E. Chaniotakis, and C. Antoniou. Shared Autonomous Vehicle Services: A Comprehensive Review. *Transportation Research Part C: Emerging Technologies*, Vol. 111, 2020, pp. 255–293. https://doi.org/10.1016/j.trc.2019.12.008.
3. Lin, Y. *Research on the Optimal Deployment of Dedicated Connected Autonomous Vehicle Lanes*. PhD thesis. Jilin University, Changchun, China, 2021.
4. Gungor, O. E., and I. L. Al-Qadi. Wander 2D: A Flexible Pavement Design Framework for Autonomous and Connected Trucks. *International Journal of Pavement Engineering*, Vol. 23, No. 1, 2020, pp. 121–136. https://doi.org/10.1080/10298436.2020.1735636.
5. Chen, F., R. Balieu, and N. Kringos. Potential Influences on Long-Term Service Performance of Road Infrastructure by Automated Vehicles. *Transportation Research Record: Journal of the Transportation Research Board*, 2016. 2550: 72–79.
6. Chen, F., M. Song, X. Ma, and X. Zhu. Assess the Impacts of Different Autonomous Trucks' Lateral Control Modes on Asphalt Pavement Performance. *Transportation Research Part C: Emerging Technologies*, Vol. 103, 2019, pp. 17–29. https://doi.org/10.1016/j.trc.2019.04.001.

7. Georgouli, K., and C. Plati. Autonomous Trucks' (ATs) Lateral Distribution and Asphalt Pavement Performance. *International Journal of Pavement Engineering*, 2022. https://doi.org/10.1080/10298436.2022.2046274.
8. Yeganeh, A., B. Vandoren, and A. Pirdavani. The Effects of Automated Vehicles Deployment on Pavement Rutting Performance. *Proc., International Airfield and Highway Pavements Conference 2021*, American Society of Civil Engineers, Reston, VA, June 8–10, 2021, pp. 280–292.
9. Zhou, F., S. Hu, S. T. Chrysler, Y. Kim, I. Damnjanovic, A. Talebpour, and A. Espejo. Optimization of Lateral Wandering of Automated Vehicles to Reduce Hydroplaning Potential and to Improve Pavement Life. *Transportation Research Record: Journal of the Transportation Research Board*, 2019. 2673: 81–89.
10. Chen, F., M. Song, and X. Ma. A Lateral Control Scheme of Autonomous Vehicles Considering Pavement Sustainability. *Journal of Cleaner Production*, Vol. 256, 2020, p. 120669. https://doi.org/10.1016/j.jclepro.2020.120669.
11. Gungor, O. E., and I. L. Al-Qadi. All for One: Centralized Optimization of Truck Platoons to Improve Roadway Infrastructure Sustainability. *Transportation Research Part C: Emerging Technologies*, Vol. 114, 2020, pp. 84–98. https://doi.org/10.1016/j.trc.2020.02.002.
12. Gungor, O. E., R. She, I. L. Al-Qadi, and Y. Ouyang. One for All: Decentralized Optimization of Lateral Position of Autonomous Trucks in a Platoon to Improve Roadway Infrastructure Sustainability. *Transportation Research Part C: Emerging Technologies*, Vol. 120, 2020, p. 102783. https://doi.org/10.1016/j.trc.2020.102783.
13. Xiaoxiang, M., T. Zhimin, and C. Feng. A Reliability-Based Approach to Evaluate the Lateral Safety of Truck Platoon Under Extreme Weather Conditions. *Accident Analysis and Prevention*, Vol. 174, 2022, p. 106775. https://doi.org/10.1016/j.aap.2022.106775.
14. Jiang, Y., L. Shen, Z. Liu, and S. Liu. A Study on the Reasonable Value for Narrowing the Width of Motor Vehicle Lane. *City Planning Review*, Vol. 46, No. 2, 2022, pp. 62–70.
15. Jiang, L., X. Zhao, J. Zhou, Y. Huang, Z. Hou, and J. Huang. Study on the Width of Vehicle Lane in Wuhan Urban Road. *Urban Roads Bridges & Flood Control*, Vol. 5, 2007, pp. 83–86. https://doi.org/10.16799/j.cnki.csdqyfh.200 7.05.019.
16. Zhang, X., and W. Zhang. Study on Lane Width of Main Line in Expressway Confluence Area Considering Safety. *Journal of Huazhong University of Science and Technology. Nature Science*, Vol. 49, No. 6, 2021, pp. 26–30.
17. Balsom, M., F. R. Wilson, and E. Hildebrand. Impact of Wind Forces on Heavy Truck Stability. *Transportation Research Record: Journal of the Transportation Research Board*, 2006, 1969: 115–120.
18. Ma, L., W.-S. Han, B.-H. Ji, and J.-X. Liu. Probability of Overturning for Vehicles Moving on a Bridge Deck in a Wind Environment Considering Stochastic Process Characteristics of Excitations. *Journal of Performance of Constructed Facilities*, Vol. 29, No. 1, 2015. https://doi.org/10.1061/(ASCE)CF.1943-5509.0000479.
19. Yuan, Z., H. Lu, L. Lin, X. Lin, and X. Gao. Study on Crosswind Stability of Van Truck on Sea-Crossing Bridge. *Automotive Engineering*, Vol. 43, No. 8, 2021, pp. 1238–1247.
20. Abd, D. M. M., T. M. M. Ahmed, and T. Y. Y. Ahmed. Characterization of Rutting Resistance of Warm-Modified Asphalt Mixtures Tested in a Dynamic Shear Rheometer. *Journal of the Mechanical Behavior of Materials*, Vol. 32, No. 1, 2023, p. 20220277. https://doi.org/10.1515/jmbm-2022-0277.
21. Shi, S., J. Tong, F. Chen, J. Hu, and T. Ma. Towards an Improved Prediction of Asphalt Pavement Rutting Through Thermal-Mechanical Coupled Constitutive Modelling. *International Journal of Pavement Engineering*, Vol. 24, No. 1, 2023, p. 2192495. https://doi.org/10.1080/10298436.2023.2192495.
22. Gungor, O. E., I. L. Al-Qadi, A. Gamez, and J. A. Hernandez. In-Situ Validation of Three-Dimensional Pavement Finite Element Models. *Proc., The Roles of Accelerated Pavement Testing in Pavement Sustainability*, Springer, Cham, 2016, pp. 145–159.
23. Siddharthan, R. V., M. Nasimifar, X. Tan, and E. Y. Hajj. Investigation of Impact of Wheel Wander on Pavement Performance. *Road Materials and Pavement Design*, Vol. 18, No. 2, 2017, pp. 390–407. https://doi.org/10.1080/14680629.2016.1162730.
24. Li, H., X. Huang, J. Zhang, and G. Liao. Rutting Simulation Analysis of Asphalt Pavement Based on Continuous Temperature Variation. *Journal of Southeast University (Natural Science Edition)*, Vol. 5, 2007, pp. 915–920. https://doi.org/10.3321/j.issn:1001-0505.2007.05.035.
25. Darabi, M. K., R. K. Abu Al-Rub, E. A. Masad, and D. N. Little. Constitutive Modeling of Fatigue Damage Response of Asphalt Concrete Materials with Consideration of Micro-Damage Healing. *International Journal of Solids and Structures*, Vol. 50, No. 19, 2013, pp. 2901–2913. https://doi.org/10.1016/j.ijsolstr.2013.05.007.
26. Ban, H., S. Im, and Y.-R. Kim. Nonlinear Viscoelastic Approach to Model Damage-Associated Performance Behavior of Asphaltic Mixture and Pavement Structure. *Canadian Journal of Civil Engineering*, Vol. 40, No. 4, 2013, pp. 313–323. https://doi.org/10.1139/cjce-2012-0289.
27. Misra, A., and V. Singh. Thermomechanics-Based Nonlinear Rate-Dependent Coupled Damage-Plasticity Granular Micromechanics Model. *Continuum Mechanics and Thermodynamics*, Vol. 27, No. 4–5, 2015, pp. 787–817. https://doi.org/10.1007/s00161-014-0360-y.
28. Zheng, M., L. Han, Z. Qiu, H. Li, Q. Ma, and F. Che. Simulation of Permanent Deformation in High-Modulus Asphalt Pavement Using the Bailey-Norton Creep Law. *Journal of Materials in Civil Engineering*, Vol. 28, No. 7, 2016. https://doi.org/10.1061/(ASCE)MT.1943-5533.0001511.
29. Ali, B., M. Sadek, and I. Shahrour. Finite-Element Model for Urban Pavement Rutting: Analysis of Pavement Rehabilitation Methods. *Journal of Transportation Engineering*, Vol. 135, No. 4, 2009, pp. 235–239. https://doi.org/10.1061/(ASCE)0733-947X(2009)135:4(235).

30. Fang, H. B., J. E. Haddock, T. D. White, and A. J. Hand. On the Characterization of Flexible Pavement Rutting Using Creep Model-Based Finite Element Analysis. *Finite Elements in Analysis and Design*, Vol. 41, No. 1, 2004, pp. 49–73. https://doi.org/10.1016/j.finel.2004.03.002.
31. Yeganeh, A., B. Vandoren, and A. Pirdavani. Impacts of Load Distribution and Lane Width on Pavement Rutting Performance for Automated Vehicles. *International Journal of Pavement Engineering*, Vol. 23, No. 12, 2022, pp. 4125–4135. https://doi.org/10.1080/10298436.2021.1935938.
32. Su, W., and R. He. Analysis and Research on Asphalt Pavement Paving and Rolling Time Based on Abaqus. *Journal of China & Foreign Highway*, Vol. 41, No. 4, 2021, pp. 58–63. https://doi.org/10.14048/j.issn.1671-2579.2021.04.012.
33. Barber, E. Calculation of Maximum Pavement Temperatures from Weather Reports. *Highway Research Board Bulletin*, No 168, 1957, pp. 1–8.
34. Gu, X., X. Liang, and Q. Dong. Numerical Simulation of Long Term Pavement Temperature Field. *Proc., International Conference: Transportation Geotechnics and Pavement Engineering*, Shanghai, 2018.
35. Zhang, L., Y. Luo, X. Chen, and R. Yang. Temperature Field Characters and Numerical Simulation of Asphalt Overlay Structure upon Previous Cement Pavement Surface. *Journal of Highway and Transportation Research and Development*, Vol. 36, No. 5, 2019, pp. 11–19.
36. Feng, D., W. Hu, F. Yu, P. Cao, and X. Zhang. Impact of Asphalt Pavement Thermophysical Property on Temperature Field and Sensitivity Analysis. *Journal of Highway and Transportation Research and Developmen*t, Vol. 28, No. 11, 2011, pp. 12–19.
37. Abu Al-Rub, R. K., M. K. Darabi, C.-W. Huang, E. A. Masad, and D. N. Little. Comparing Finite Element and Constitutive Modelling Techniques for Predicting Rutting of Asphalt Pavements. *International Journal of Pavement Engineering*, Vol. 13, No. 4, 2012, pp. 322–338. https://doi.org/10.1080/10298436.2011.566613.
38. Song, M., and F. Chen. The Influence of Autonomous Vehicles on Asphalt Pavement's Service Life and Maintenance Cost. *China Journal of Highway and Transport*, 2021. https://kns.cnki.net/kcms/detail/61.1313.U.20211109.1553.004.html.
39. Huang, W.-J., and N.-C. Su. A Study of Generalized Normal Distributions. *Communications in Statistics: Theory and Methods*, Vol. 46, No. 11, 2017, pp. 5612–5632. https://doi.org/10.1080/03610926.2015.1107585.
40. Qu, D., Y. Zhou, B. Su, and Z. Sun. The Study of the Effect of Urban Road Traffic Capacity with Lane Occupied. *Proc., 27th Chinese Control and Decision Conference (CCDC)*, Qingdao, China, IEEE, New York, May 23–25, 2015, pp. 5122–5127.
41. Zhu, F., and S. V. Ukkusuri. Modeling the Proactive Driving Behavior of Connected Vehicles: A Cell-Based Simulation Approach. *Computer-Aided Civil and Infrastructure Engineering*, Vol. 33, No. 4, 2018, pp. 262–281. https://doi.org/10.1111/mice.12289.
42. Zhu, Y. *Research on Design Controlling Index for Semi-rigid Base Asphalt*. PhD thesis. Southeast University, Nanjing, Jiangsu, China, 2019.
43. Ma, T., G. Liao, and X. Huang. *Application of Abaqus Finite Element Software in Road Engineering*, 3rd ed. Southeast University Press, Nanjing, 2021.
44. Li, S., M. Fan, L. Xu, W. Tian, H. Yu, and K. Xu. Rutting Performance of Semi-Rigid Base Pavement in RIOHTrack and Laboratory Evaluation. *Frontiers in Materials*, Vol. 7, 2021, p. 590604. https://doi.org/10.3389/fmats.2020.590604.
45. Zhou, D., Z. Zhou, and J. Liu. Comparative Studies on Laboratory Rutting Test and Evaluating Indicator of Asphalt Concrete. *Journal of Rail Way Science and Engineering*, Vol. 19, No. 8, 2022, pp. 2287–2294.
46. Kanaan, A. I., H. Ozer, and I. L. Al-Qadi. Testing of Fine Asphalt Mixtures to Quantify Effectiveness of Asphalt Binder Replacement Using Recycled Shingles. *Transportation Research Record: Journal of the Transportation Research Board*, 2014. 2445: 103–112.
47. Fang, H. *Permanent Deformation Behavior of Asphalt and Asphalt Mixtures and Its Simulation Analysis*. PhD thesis. Wuhan University of Technology, China, 2018.
48. Lu, Y., L. Tian, Y. Kou, and C. Sun. Analysis of Vehicle Speed Characteristics of Urban Road Based on Axle Map. *Journal of Nanjing University of Science and Technology*, Vol. 44, No. 4, 2020, pp. 488–492.
49. Zhang, Z., X. Hao, W. Wu, and D. Wang. The Running Speed Prediction Model of Interchange Ramp. *Journal of Transportation Systems Engineering & Information Technology*, Vol. 15, No. 1, 2015, pp. 93–99.